Sub-cycle Phase Angle-Oriented Algorithm for Identifying Fault Direction in Renewable-Rich MV Distribution Grids

Tajdinian, Mohsen; Behdani, Behzad; Hoq, Md Tanbhir; Popov, Marjan

DOI
10.1109/TIM.2024.3460879

Publication date
2024

Document Version
Final published version

Published in
IEEE Transactions on Instrumentation and Measurement

Citation (APA)
Tajdinian, M., Behdani, B., Hoq, M. T., & Popov, M. (2024). Sub-cycle Phase Angle-Oriented Algorithm for Identifying Fault Direction in Renewable-Rich MV Distribution Grids. *IEEE Transactions on Instrumentation and Measurement*, *73*, Article 9005211. https://doi.org/10.1109/TIM.2024.3460879

Sub-Cycle Phase Angle-Oriented Algorithm for Identifying Fault Direction in Renewable-Rich MV Distribution Grids

Mohsen Tajdinian, Behzad Behdani, *Member, IEEE*, Md Tanbhir Hoq, and Marjan Popov, *Fellow, IEEE*

***Abstract*— The integration of renewable energy sources has significantly impacted power system protection schemes, primarily by increasing short-circuit fault currents, which, in turn, raises the possibility of current transformer (CT) saturation, and by introducing bidirectional fault current flow, which interferes with the directional selectivity of relays in detecting downstream faults. This study presents a novel fault direction identification algorithm aimed at immunization against CT saturation effects, especially in medium voltage (MV) distribution grids integrated with renewable sources. To achieve this, two distinct computational frameworks have been developed and proposed. The first framework utilizes the modified least squares (MLSs) method, while the second employs a modified Kalman filter (MKF). Both algorithms calculate the fundamental current phase angle using a sub-cycle window of current samples, ensuring resilience to heavily distorted waveforms caused by CT saturation, even under conditions of deep saturation. The effectiveness of the proposed method is validated through numerous tests conducted on fault currents recorded via simulation scenarios and field measurements, considering various fault inception times, resistances, and locations, together with different neutral grounding arrangements. Comparative assessments of the two developed frameworks across different scenarios indicate that both methods exhibit promising performances, although the least square-based method demonstrates superior efficiency compared to the Kalman filter-based method.**

***Index Terms*— Current transformer (CT) saturation, directional relay, Kalman filter, least squares (LSs), protection.**

I. Introduction

BIDIRECTIONAL medium voltage (MV) distribution grids with dispersed generations (DGs) pose challenges to conventional protection schemes in deregulated radial distribution MV distribution grids [1]. While meshed structures enhance the reliability of power grids, they introduce complexities to protection schemes due to multiple sources contributing to fault current signals [2]. Consequently, fault direction becomes variable, depending on factors such as fault location (FL), generator size, and power system structure [3], [4]. Changes in fault current may cause current-dependent protective relays (e.g., distance and overcurrent relays) to malfunction for out-of-zone faults [5]. Hence, directionally selective schemes are necessary for networks with multiple sources and meshed structures to improve sensitivity and security through fault direction identification [6]. Concerning the domain of analysis, the published directional algorithms are categorized as follows.

1) *Time domain (TD) algorithms [7], [8], [9], [10]:* These algorithms operate based on computations utilizing voltage and/or current signals. In [7], the superimposed components technique was employed for measured voltage signals to discriminate fault direction. The sign of correlogram function applied to pre- and postfault current signals was proposed as fault direction detection criteria in [8]. A directional algorithm based on the rate of change of current over time was presented in [9]. In [10], the instantaneous frequency calculated from the current signal was utilized as a directional index. Generally, TD algorithms have low response delays (less than 5 ms) and introduce less computational burden in comparison with other techniques. However, these methods require threshold readjustment to properly operate for different power systems.
2) *Frequency domain (FD) algorithms [11], [12], [13]:* These algorithms are developed based on variations in phasor components of currents and/or voltages. The method in [11] is developed based on the variations in amplitudes of measured fundamental current and voltage components. The symmetrical components are utilized for fault direction detection in [12] and [13], where the former employs the negative sequence current, and the latter applies the sequence current amplitude along with sequence phase angle as directional criteria. These methods are less sensitive to noise and fault transients compared with TD algorithms. However, these algorithms mostly introduce a full cycle delay, as the required phase angles are computed by discrete Fourier transform (DFT).
3) *Time-FD (TFD) algorithms [14], [15], [16], [17]:* These algorithms operate based on the features extracted from measured current and/or voltage signals. A protection

Received 22 March 2024; revised 24 July 2024; accepted 20 August 2024. Date of publication 16 September 2024; date of current version 25 September 2024. This work was supported in part by Nederlandse Organisatie voor Wetenschappelijk Onderzoek (NWO) through the Project "Protection of Future Power System Components (PRoteuS)" under Grant 18699. The Associate Editor coordinating the review process was Dr. Marco Pau. *(Corresponding author: Behzad Behdani.)*

Mohsen Tajdinian and Md Tanbhir Hoq are with the Hitachi Energy Research, 72226 Västerås, Sweden (e-mail: mohsen.tajdinian@hitachienergy.com; md-tanbhir.hoq1@hitachienergy.com).

Behzad Behdani and Marjan Popov are with the Faculty of Electrical Engineering, Mathematics and Computer Science, Delft University of Technology, 2628 CD Delft, The Netherlands (e-mail: b.behdani-1@tudelft.nl; m.popov@tudelft.nl).

Digital Object Identifier 10.1109/TIM.2024.3460879

TABLE I
SUMMARIZING THE FEATURES OF DIRECTION RELAY ALGORITHMS

Method Category		TD [7]–[10]	FD [11]–[13]	TFD [14]–[17]	AI [19]–[21]
Input	Current-Only	✓	✗	✗	✗
	Voltage & Current	✓	✓	✓	✓
Response Time (Cycle)		∼ 1/4	∼ 1	∼ 1/4	∼ 1/2
Sampling Frequency		Low	∼ Low	High	∼ Low
Noise Sensitivity		∼ Low	Low	High	Medium
Complexity		Low	Low	Medium	High

∼ Approximately

logic was proposed in [14] by employing wavelet transform to extract fault transient signatures. The initial arrival of fault traveling wave was identified by wavelet transform and utilized as the directional index in [15]. A similar approach was proposed in [16], where a directional detection criterion was developed based on the traveling wave polarity calculated from the synchrosqueezing transform. The signatures of fault traveling waves extracted by S-Transform were applied in another application to determine the fault zone in an HVDC converter station [17]. TFD algorithms are widely applied for other critical power system protection schemes as well [18]. Compared with other groups, these algorithms show faster responses. However, their requirements for high sampling rates and high sensitivity to noise are the main drawbacks of the TFD algorithms.

4) *Artificial intelligent algorithms [19], [20], [21]:* These algorithms utilize AI networks trained based on features on the current and/or voltage signals to determine fault direction. In [19], a neural network (NN) trained by features extracted by wavelet transform was proposed. A modular NN was proposed as a directional relay algorithm in [20], while [21] presents a multilayer feedforward NN for this task. The models built on AI algorithms have been proposed for different protection strategies in power systems [22]. Although for their quick and highly accurate responses, these methods demand huge training datasets, considerable computational time to build the model, and also require retraining to rebuild the model upon network topology changes, marking the main drawbacks of these algorithms.

State-of-the-art directional protection algorithms can be compared based on various factors, including the type of input signals, response time, sampling frequency, noise sensitivity, and complexity, as summarized in Table I. From Table I, it is evident that TD algorithms exhibit superiority over other approaches. However, it should be noted that while TD algorithms offer advantages, they are not completely immune to signal distortions. This is particularly critical for current-only algorithms, which are susceptible to current transformer (CT) saturation. With the integration of renewable energy resources (RESs) into MV distribution grids, the likelihood of CT saturation due to enhanced short-circuit faults has increased significantly.

Additionally, RESs may introduce transient components into fault currents, which have not been thoroughly studied previously. It has been acknowledged that in the case of a short circuit close to a rotational generator [i.e., synchronous generator (SG) or induction generator (IG), doubly fed IG (DFIG)], the sinusoidal component of fault current does not remain constant-magnitude and may vary in time. The main reason is that in a fault close to the terminal of a rotational generator, the flux is not constant, and it starts to change [23]. These changes are reflected in voltage and current magnitudes as time-variant terms. Apart from the magnitude, the frequency can also vary, especially for IGs and DFIGs [23]. More specifically, when a fault happens, high currents can damage the converters, and therefore, crowbar operation is provided to limit the short circuit current. If, due to a short-circuit fault, the crowbar protection is activated, the stator fault current of DFIGs would behave similar to IGs [24], [25]. In such a condition, not only would the magnitude of the stator current exhibit time-variant behavior, but its frequency would also vary due to the slip variation. As a result of these transient behaviors in RESs, the directional algorithms may operate with large delays or even incorrectly [9], [10].

Consequently, the rapid identification of fault direction and maintaining detection immunity to CT saturation pose challenges for current-only directional algorithms, especially for deregulated MV distribution grids.

To effectively address the challenges outlined, this article presents two efficient fault direction identification frameworks tailored for numerical relays considering the challenges in renewable-rich MV power distribution grids. These frameworks are built on the principle of sub-cycle calculation of the fundamental current component's phase angle, categorizing them under FD directional relay algorithms. The following highlights the contributions of this article.

1) Depending on the fault condition, the fault current may contain asymmetrical decaying dc offset, which can introduce substantial oscillations to the estimated fundamental current phase angle. To mitigate the influence of the decaying dc offset, a series of analytical formulations are introduced to estimate its time constant. These formulations, as demonstrated, require less than five samples (considering 100 samples/cycle sampling rate and nominal frequency 50 Hz) for accurate estimation. It is important to note that the estimated time constant will be utilized in the subsequent stage to estimate the fundamental current phase angle.
2) With the time constant determined and accounting for the presence of an exponentially decaying dc component, the phase angle of the fundamental current component is estimated using the following two frameworks.
    a) The first framework introduces a modified sliding window least squares (LSs) technique designed to estimate the phase angle of the fundamental current component within a sub-cycle time frame.
    b) The second algorithm employs a Kalman filter to derive the phase angle of the fundamental current component. Due to its recursive nature, the Kalman filter ensures minimal computational burden and

requires only a minimum amount of sampling data for accurate estimation.

3) The proposed algorithms require only a minimum number of current samples to estimate accurately the phase angle of the fundamental current component. As a result, they exhibit strong immunity to CT saturation effects during faults.
4) Given that CT saturation effects typically occur within the first cycle, the proposed sub-cycle method is complemented by a CT saturation detection criterion. This criterion calculates phase angle differences to verify the accuracy of the phase angle provided to the directional relay. In nonsaturated intervals, the difference is nearly zero, while during saturation, the difference becomes significant, allowing the criterion to detect saturation.

The rest of the article contains the following: Section II describes the mathematical basis of the proposed algorithms. Section III provides the directional relay criteria and implementation. Sections IV–VI contain the simulation and experimental results with the performance comparison and discussions. Finally, Section VII concludes the achievements of the proposed algorithms.

II. Proposed Algorithms

To calculate the fundamental phase angle, a two-stage algorithm is developed. In the first stage, the dc component is removed through derivative-based formulations and time-constant estimation. In the second stage, the proposed algorithm calculates the fundamental current component's phase angle via either of two frameworks, i.e., the modified least square (MLS) technique or the modified Kalman filter (MKF). Eventually, the fundamental phase angle is sent to the directional relay criteria for decision-making on the fault direction.

A. Time Constant Estimation

Fault current may be contaminated with an exponentially decaying dc component, showing asymmetrical behavior. Under the fault condition, the current signal is represented as follows:

$$i(t) = I_{\mathrm{dc}} e^{-t/\tau_{\mathrm{dc}}} + I_m \cos(2\pi f_0 t + \alpha) \tag{1}$$

where I_m, α, and f_0 are the magnitude, phase angle, and frequency of the fundamental component, respectively. Besides, I_{dc} and τ_{dc} are the magnitude and time constant of the exponentially decaying dc component, respectively. It is important to note in digital protective relays or intelligent electronic devices (IEDs), the system frequency is monitored by a preprocessing block for different applications, including fault detection, and impedance calculations. Similar to any other frequency-dependent algorithms, the computations of the proposed methods are carried out by receiving the nominal frequency as an input. By calculating the first, second, and third derivatives of (1), the following expressions are obtained:

$$\frac{di(t)}{dt} = -\frac{I_{\mathrm{dc}} e^{-t/\tau_{\mathrm{dc}}}}{\tau_{\mathrm{dc}}} - 2\pi f_0 I_m \sin(2\pi f_0 t + \alpha) \tag{2}$$

$$\frac{d^2 i(t)}{dt^2} = \frac{I_{\mathrm{dc}} e^{-t/\tau_{\mathrm{dc}}}}{(\tau_{\mathrm{dc}})^2} - (2\pi f_0)^2 I_m \cos(2\pi f_0 t + \alpha) \tag{3}$$

$$\frac{d^3 i(t)}{dt^3} = -\frac{I_{\mathrm{dc}} e^{-t/\tau_{\mathrm{dc}}}}{(\tau_{\mathrm{dc}})^3} + (2\pi f_0)^3 I_m \sin(2\pi f_0 t + \alpha). \tag{4}$$

By applying some mathematical manipulations and simplifications on (2)–(4), the expression in (5), as shown at the bottom of the next page, can be concluded.

Simplifying expression (5), the time constant is estimated as follows:

$$\tau_{\mathrm{dc}} = \left| \frac{\dfrac{d^2 i(t)}{dt^2} + (2\pi f_0)^2 i(t)}{\dfrac{d^3 i(t)}{dt^3} + (2\pi f_0)^2 \dfrac{di(t)}{dt}} \right|. \tag{6}$$

For simplicity, the formulations to calculate the time constant are derived in continuous form. It is worth noting that in practice and during implementation, the first, second, and third order of derivations is approximated using backward difference. This means at least five samples of current signals are required to estimate the time constant.

B. Least Square-Based Phase Angle Calculation

The fault current expression (1) can be rewritten in the form of (7). Considering that the time delay is calculated by (6), three unknown variables, i.e., I_m, α, and I_{dc} remain. Fault current can be expanded and expressed discretely as follows:

$$i(n) = I_{\mathrm{dc}} e^{-nT_s/\tau_{\mathrm{dc}}} + I_m \cos(\alpha)\cos(2\pi f_0 n\mathrm{T}_s) - I_m \sin(\alpha)\sin(2\pi f_0 n\mathrm{T}_s). \tag{7}$$

Taking the effect of noise vector $\boldsymbol{v}$ into consideration, (7) can be rewritten in matrix form for n consecutive samples as follows:

$$\boldsymbol{I}_i^{n\times 1} = \boldsymbol{I}_s^{n\times 3} \times \boldsymbol{I}_x^{3\times 1} + \boldsymbol{v}^{n\times 1} \tag{8}$$

$$\boldsymbol{I}_i^{n\times 1} = [i(1) \quad i(2) \quad i(3) \quad \ldots m \quad i(nT_s)]^{\mathrm{T}} \tag{9}$$

$$\boldsymbol{I}_x^{3\times 1} = [I_{\mathrm{dc}} \quad I_m \cos(\alpha) \quad I_m \sin(\alpha)]^{\mathrm{T}} \tag{10}$$

$$\boldsymbol{I}_s^{n\times 3} = \begin{bmatrix} e^{-\mathrm{T}_s/\tau_{\mathrm{dc}}} & \cos(2\pi f_0 \mathrm{T}_s) & -\sin(2\pi f_0 \mathrm{T}_s) \\ e^{-2\mathrm{T}_s/\tau_{\mathrm{dc}}} & \cos(2\pi f_0 2\mathrm{T}_s) & -\sin(2\pi f_0 2\mathrm{T}_s) \\ e^{-\mathrm{T}_s/\tau_{\mathrm{dc}}} & \cos(2\pi f_0 3\mathrm{T}_s) & -\sin(2\pi f_0 3\mathrm{T}_s) \\ \vdots & \vdots & \vdots \\ e^{-nT_s/\tau_{\mathrm{dc}}} & \cos(2\pi f_0 nT_s) & -\sin(2\pi f_0 nT_s) \end{bmatrix}. \tag{11}$$

The LS technique is a reliable and fast solution for (8), which is able to estimate unknown parameters $\boldsymbol{I}_x$ such that the sum of squares of noise terms (errors) in $\boldsymbol{v}$ are minimized. Yielding this condition, the unknown states are estimated as [26]

$$\boldsymbol{I}_x = \left(\boldsymbol{I}_s^{\mathrm{T}} \boldsymbol{I}_s\right)^{-1} \boldsymbol{I}_s^{\mathrm{T}} \boldsymbol{I}_i \tag{12}$$

where T is a transpose notation. At each current sample, the fundamental current phase angle (α) is obtained using (10) as follows:

$$\alpha(n) = \tan^{-1}\left(-\frac{\boldsymbol{I}_x(3)}{\boldsymbol{I}_x(2)}\right). \tag{13}$$

C. Kalman Filter-Based Phase Angle Calculation

The Kalman filter is a powerful tool for state estimation in power systems [27], and here, it is employed to estimate the fundamental current component's phase angle as

$$\boldsymbol{I}_x(n+1) = \boldsymbol{\Phi}(n)\boldsymbol{I}_x(n) + \boldsymbol{\Gamma}(n)\boldsymbol{w}(n) \tag{14}$$

$$\boldsymbol{I}_i(n) = \boldsymbol{I}_s(n)\boldsymbol{I}_x(n) + \boldsymbol{\varepsilon}(n) \tag{15}$$

where according to (7)

$$\boldsymbol{I}_x(n) = [I_{\mathrm{dc}} \quad I_m\cos(\alpha) \quad I_m\sin(\alpha)]^{\mathrm{T}} \tag{16}$$

$$\boldsymbol{\Phi}(n) = \mathbb{I}^{3\times 3} \tag{17}$$

$$\boldsymbol{I}_s(n) = \left[e^{-nT_s/\tau_{\mathrm{dc}}} \quad \cos(2\pi f_0 nT_s) \quad -\sin(2\pi f_0 nT_s)\right] \tag{18}$$

where $\mathbb{I}$ denotes identity matrix and (14) and (15) are corresponding to the state variable $\boldsymbol{I}_x(n)$ and the measured samples $\boldsymbol{I}_i(n)$. Notice that $\boldsymbol{\Phi}(n)$ and $\boldsymbol{I}_s(n)$ are transition and measurement matrices, respectively. The terms $\boldsymbol{w}(n)$ and $\boldsymbol{\varepsilon}(n)$ are state noise and measurement error with covariance matrices $\boldsymbol{Q}$ and $\boldsymbol{R}$, respectively. Here, it is assumed there is no random input, meaning $\boldsymbol{w}(n)$ is zero, and thus, $\boldsymbol{Q} = \boldsymbol{0}$ [28]. On the other hand, $\boldsymbol{R}$ is calculated as suggested in [29], where the system output is held constant, and the noise effect is extracted by first removing its mean from the data and then calculating the covariance from the residual data.

Kalman filter [28], assumes an initial value for state variables $\boldsymbol{I}_x(n)$, and as each sample of the current signal becomes available, the state variable is recursively updated. The recursive calculation is mathematically expressed as follows:

$$\begin{aligned}\boldsymbol{I}_x(n+1) = {} & \boldsymbol{\Phi}(n)\boldsymbol{I}_x(n) + \boldsymbol{K}(n+1)\boldsymbol{I}_i(n+1) \\ & - \boldsymbol{K}(n+1)\boldsymbol{I}_s(n+1)\boldsymbol{\Phi}(n)\boldsymbol{I}_x(n).\end{aligned} \tag{19}$$

The recursive calculation in (19) requires calculating the gain matrix $\boldsymbol{K}$. To calculate the gain matrix $\boldsymbol{K}$, first, the covariance matrix $\boldsymbol{P}$ should be updated as follows:

$$\boldsymbol{P}(n+1|n) = \boldsymbol{\Phi}(n)\boldsymbol{P}(n|n)\boldsymbol{\Phi}^{\mathrm{T}}(n) + \boldsymbol{\Gamma}(n)\boldsymbol{Q}(n)\boldsymbol{\Gamma}^{\mathrm{T}}(n) \tag{20}$$

where T denotes the transpose of the matrix. As mentioned above, since there is no random input to the system, the term related to $\boldsymbol{Q}$ is disregarded. Using (20), the gain matrix is updated as follows:

$$\begin{aligned}\boldsymbol{K}(n+1) = {} & \boldsymbol{P}(n+1|n)\boldsymbol{I}_s^{\mathrm{T}}(n+1) \\ & \times \left[\boldsymbol{I}_s(n+1)\boldsymbol{P}(n+1|n)\boldsymbol{I}_s^{\mathrm{T}}(n+1) + \boldsymbol{R}_{k+1}\right]^{-1}.\end{aligned} \tag{21}$$

For the next iteration, covariance matrix $\boldsymbol{P}$ is updated as

$$\boldsymbol{P}(n+1|n+1) = [\mathbb{I} - \boldsymbol{K}(n+1)\boldsymbol{I}_s(n+1)]\boldsymbol{P}(n+1|n). \tag{22}$$

At each current sample, the fundamental current component's phase angle (α) is obtained using (18) as follows:

$$\alpha(n) = \tan^{-1}\left(-\frac{\boldsymbol{I}_x(3)}{\boldsymbol{I}_x(2)}\right). \tag{23}$$

It should be noted that $\boldsymbol{I}_i$, $\boldsymbol{I}_x$, and $\boldsymbol{I}_s$ have the same role for both least square and Kalman filter phase angle estimation.

D. Fourier Transform-Based Phase Angle Calculation

The DFT algorithm is one of the most straightforward mathematical methods applied for frequency-domain analysis, especially in power system protection [28]. This algorithm is widely used for extracting fundamental phasor components in power systems. To extract the real and imaginary parts of the fault current signal in (1), the DFT algorithm is applied as follows:

$$I_{\mathrm{Re}} = \sum_{n=1}^{k} i(n)\sin\left(\frac{2\pi f_0 n\mathrm{T}_s}{k}\right) \tag{24}$$

$$I_{\mathrm{Im}} = \sum_{n=1}^{k} i(n)\cos\left(\frac{2\pi f_0 n\mathrm{T}_s}{k}\right) \tag{25}$$

where I_{Re} and I_{Im} denote the real and imaginary parts of the fault current, respectively, T_s is the sampling time, and k is the total number of samples in one cycle.

Using the real and imaginary parts of the fault current calculated by the DFT algorithm according to expressions (24) and (25), the fundamental phasor component of the fault current ($I_m \sphericalangle \alpha$) can be obtained as

$$I_m = \sqrt{I_{\mathrm{Re}}^2 + I_{\mathrm{Im}}^2} \tag{26}$$

$$\alpha = \tan^{-1}\left(\frac{I_{\mathrm{Im}}}{I_{\mathrm{Re}}}\right). \tag{27}$$

In this article, the DFT algorithm is used as a basis to evaluate the performances of the proposed MLS and MKF-based frameworks.

III. Directional Relay Criteria and Implementation

The directional relay criterion (DRC) is based on the variation of the fundamental phase angle and is defined

$$\begin{aligned}\frac{\dfrac{d^2 i(t)}{dt^2} + (2\pi f_0)^2 i(t)}{\dfrac{d^3 i(t)}{dt^3} + (2\pi f_0)^2 \dfrac{di(t)}{dt}} &= \frac{\dfrac{I_{\mathrm{dc}}e^{-t/\tau_{\mathrm{dc}}}}{(\tau_{\mathrm{dc}})^2} - (2\pi f_0)^2 I_m\cos(2\pi f_0 t + \alpha) + (2\pi f_0)^2(I_{\mathrm{dc}}e^{-t/\tau_{\mathrm{dc}}} + I_m\cos(2\pi f_0 t + \alpha)}{-\dfrac{I_{\mathrm{dc}}e^{-t/\tau_{\mathrm{dc}}}}{(\tau_{\mathrm{dc}})^3} + (2\pi f_0)^3 I_m\sin(2\pi f_0 t + \alpha) + (2\pi f_0)^2\left(-\dfrac{I_{\mathrm{dc}}e^{-t/\tau_{\mathrm{dc}}}}{\tau_{\mathrm{dc}}} - 2\pi f_0 I_m\sin(2\pi f_0 t + \alpha)\right)} \\ &= \frac{\dfrac{I_{\mathrm{dc}}e^{-t/\tau_{\mathrm{dc}}}}{(\tau_{\mathrm{dc}})^2} + (2\pi f_0)^2 I_{\mathrm{dc}}e^{-t/\tau_{\mathrm{dc}}}}{-\dfrac{I_{\mathrm{dc}}e^{-t/\tau_{\mathrm{dc}}}}{(\tau_{\mathrm{dc}})^3} - (2\pi f_0)^2\dfrac{I_{\mathrm{dc}}e^{-t/\tau_{\mathrm{dc}}}}{\tau_{\mathrm{dc}}}} = -\tau_{\mathrm{dc}}\end{aligned} \tag{5}$$

as follows:

$$\mathrm{DRC}(n) = \frac{\alpha(n)}{\pi} \tag{28}$$

where $\mathrm{DRC}(n)$ is the criteria at nth sample after fault inception. Besides, to ensure the immunity of DRC to CT saturation, a condition for CT saturation detection is defined

$$\mathrm{SI}(n) = \frac{|\alpha(n) - \alpha(n-1)|}{\pi} \tag{29}$$

where $\mathrm{SI}(n)$ is the value of saturation index (SI) at nth sample. If the value of $\mathrm{SI}(n)$ exceeds a certain threshold for five consecutive samples, then saturation is detected, and new values will not be calculated for DRC that remains unchanged for the subsequent samples of current signals.

The permissible range for forward and backward faults is derived based on the following assumptions.

1) Normal power flow (NPF): is one of the factors that affect the permissible range of the fault current direction. According to the positive and negative NPF directions for the relay position, the load angle (γ) is considered to be within the interval ($-\pi/6 < \gamma < \pi/6$).
2) There are various transmission lines in a power grid with different per kilometer impedances, which affect the impedance angle (θ) and consequently the phase angle after fault inception. Here, the impedance angle (θ) is assumed to be within the range ($\pi/4 < \theta < \pi/2$) to account for both distribution lines (with low L/R ratios) and transmission lines (with high L/R ratios).

Based on previously mentioned assumptions, the phase angle after fault inception, i.e., α, will be within the following ranges corresponding to forward and backward faults.

1) *Forward:* $\alpha_f = \gamma - \theta$, resulting $-2\pi/3 < \alpha_f < -\pi/12$.
2) *Backward:* $\alpha_b = \gamma - \theta + \pi$, resulting $\pi/3 < \alpha_b < 11\pi/12$.

According to the permissible ranges for forward and backward faults, the index will be within the following ranges.

1) *Forward Fault:* $-2\pi/3 < \alpha_f < -\pi/12$, which results in $-2/3 < \mathrm{DRC}_f < -1/12$.
2) *Backward Fault:* $\pi/3 < \alpha_b < 11\pi/12$, which results in $1/3 < \mathrm{DRC}_b < 11/12$.

Fig. 1 shows the implementation procedure of the proposed directional framework. The operation zones of the proposed framework as described above are graphically depicted by the diagrams in Fig. 2. The current samples are obtained at a sampling frequency of 5 kHz corresponding to 100 samples/cycle for 50 Hz frequency. It is worth mentioning that here, for the sake of comprehensiveness, the fundamental frequency is tracked by a *Frequency Tracking Block* in MATLAB, calculating the derivative of the phase angle variation of the signal for a synchronous phasor rotating at the specified nominal frequency [30]. The proposed directional framework is detailed by the steps in Algorithm 1.

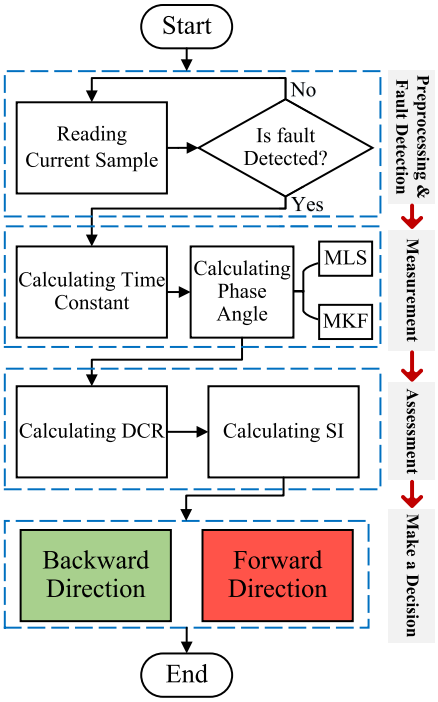

Fig. 1. Implementation procedure of the proposed directional framework.

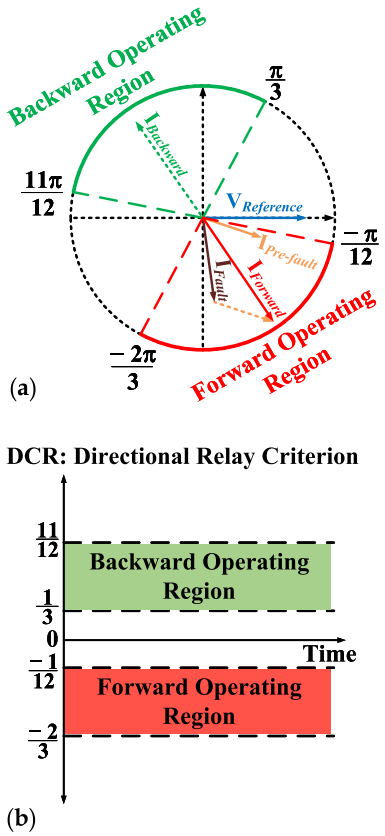

Fig. 2. General operation zones of the proposed directional framework in (a) polar plane and (b) TD.

IV. Simulation Results and Discussions

In the following, the performance of the presented directional algorithm is evaluated based on both calculation frameworks. Fig. 3 shows a modified microgrid adopted from [31], simulated in MATLAB/Simulink. The microgrid contains four DGs, including one DFIG, one IG, an inverter-based photovoltaic (PV) farm, and a SG. Detailed dynamic

Algorithm 1 Proposed Directional Framework

Input: Current sample $i(n)$
Output: Fault Direction: Forward or Backward

1. Receive $i(n)$
2. Check for fault occurrence
   if fault flag = 0
   Go to step 1
   else
3. Derive time constant τ_{dc} from (6)
4. Select a Method
   MLS: Estimate $I_m \cos(\alpha) \& I_m \sin(\alpha)$ from (8)-(12)
   Calculate phase angle $\alpha(n)$ from (13)
   MKF: Estimate $I_m \cos(\alpha) \& I_m \sin(\alpha)$ from (14)-(22)
   Calculate phase angle $\alpha(n)$ from (23)
5. Calculate DRC(n) from (28)
6. Check for Saturation using SI(n) from (29)
7. count $= 0$;
8. **if** SI(n) $\geq$ threshold
9. count $=$ count $+ 1$;
10. **if** count ≥ 5
11. DRC(n) $=$ DRC($n-1$)
12. **end if**
13. **else**
14. count $= 0$;
15. **end if**
16. **if** $-2/3 <$ DRC(n) $< -1/12$
17. Fault Direction $\leftarrow$ Forward
18. **else if** $1/3 <$ DRC(n) $< 11/12$
19. Fault Direction $\leftarrow$ Backward
20. **end if**
21. **end**
21. **return** Fault Direction

models have been implemented for all the generators, considering parameters such as the inertia constant, friction factor, and generator transient and sub-transient reactances and torques. For the inverter-based wind farm, the Type-4 detailed model in MATLAB/Simulink is applied. The power transformers are modeled considering the magnetization branch with the nonlinear saturation and hysteresis effects according to the guidelines in [32] and [33]. Additionally, PI-section models are utilized to model the distribution lines. While the general specifications of the adopted microgrid are given in Table II, the detailed parameters of the test system are provided in [31].

The main circuit breaker (CB), positioned near transformer number 1 (T#1), is employed to reproduce the grid-connected and islanded operation modes. In addition, CBs 1 and 2 can be used to change the topology from radial to loop and vice versa. Several fault scenarios, including different fault types (FTs), FLs, fault resistance (FR), and fault incipient angles (FIAs), considering different combination statuses of CBs for loop and radial in grid-connected and islanded modes are generated. The specifications for the fault and switching conditions are shown in Table III.

The directional relays are installed at the two sides of bus 5. At each side, three single-phase class 5PX CTs are applied

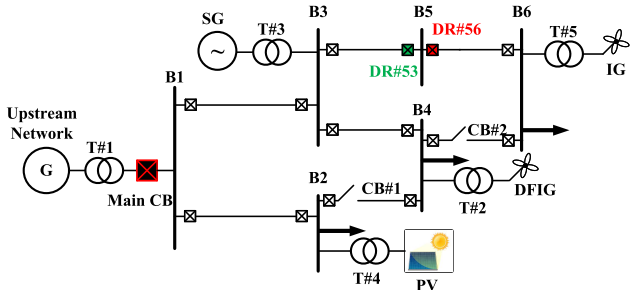

Fig. 3. Test system for performance evaluation of proposed detection index.

TABLE II
GENERAL SPECIFICATIONS OF THE ADOPTED TEST SYSTEM

Component	Parameter	Unit
Line	Positive sequence resistance	$0.0135\,\Omega$/km
	Zero sequence resistances	$0.0424\,\Omega$/km
	Positive sequence inductance	4.987×10^{-5} H/km
	Zero sequence inductance	1.39×10^{-4} H/km
	Positive sequence capacitance	11.33×10^{-9} F/km
	Zero sequence capacitance	5.01×10^{-9} F/Km
	Distance	$20 - 40$ km
Transformers	T#1: Voltage ratio	79/13 kV
	Rated apparent power	10 MVA
	T#2 & T#5: Voltage ratio	0.575/13 kV
	Rated apparent power	9 MVA
	T#3 & T#4: Voltage ratio	0.45/13 kV
	Rated apparent power	10 MVA
Generator	Upstream grid: Voltage	79 kV
	Rated apparent power	1000 MVA
	Frequency	50 Hz
	DFIG: Voltage	575 V
	Rated apparent power	1.5 MVA
	IG: Voltage	575 V
	Rated apparent power	1.5 MVA
	PV: Voltage	400 V
	Rated apparent power	10 MVA
	SG: Voltage	400 V
	Rated apparent power	6 MVA

TABLE III
CONDITIONS OF CASE STUDIES

Parameter	Range	Number
FT	LLLG, LLL, LLG, LL, LG	2000
FR	$0 - 50\,\Omega$	
FL	$0 - 100\%$ of each line	
FIA	$0 - 360^\circ$	
Gaussian Noise	30 to 50 dB	

with the turn ratio of 1200/5 and the burden capacity of 20 VA, according to the specifications given in [34]. Similar to the power transformers, the CTs are modeled considering the parameters, including winding resistances and leakage inductances, and core magnetizations and losses, along with the nonlinear effects of saturation and hysteresis according to [32] and [33]. With these CTs, the relay can measure the instantaneous values of fault currents and voltage signals

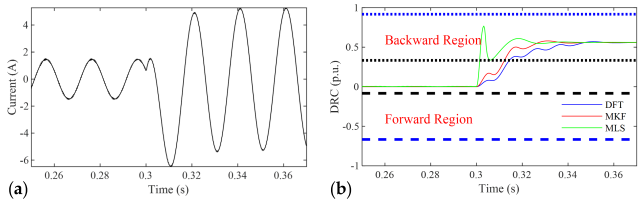

Fig. 4. Performance of the fault direction detection algorithm. (a) Fault current signal for SLG fault between buses 3 and 5. (b) Calculated DRC using different frameworks for SLG fault between buses 3 and 5.

in intervals of 1 ms. At the 50 Hz frequency, this relay can record 20 samples/cycle. Since the proposed algorithms require 100 samples/cycle, the recorded data are first resampled using the resampling function in MATLAB software and then fed to the algorithm for further processing. It is also worth noting that the adopted relay can memorize the event for 50 consecutive cycles, recorded in the *Comtrade* format, which is the standard format for protective relays.

As mentioned earlier, to demonstrate the effectiveness of the proposed algorithms more clearly, phase angles estimated by the DFT are also used as a reference and further shown in the results.

A. Faults With/Without Saturation

Fig. 4 shows waveforms from a single line to ground (SLG) fault between buses 3 and 5 with the resistance of 10 Ω, initiated at $t = 0.3$ s considering grid-islanded mode. Considering (DR#56) as the measurement reference, it can be seen in Fig. 4, that MKF and DFT identify the fault's backward direction after 14 and 16.5ms, respectively measured from fault occurrence instant at 0.3s. However, MLS identifies the fault's backward direction only 2ms after fault inception. It is deduced that MKF and DFT are more sensitive to the decaying dc compared to MLS, and thus, they introduce longer delays with respect to MLS.

For a short circuit containing CT saturation, the current signal becomes significantly distorted and deviates notably from the standard waveform of (1). The two fault signals accompanied by CT saturation are shown in Fig. 5 including a triple line to ground fault (3LG) between buses 3 and 5, initiated at $t = 0.3$ s, and a double line to ground fault (LLG) between buses 5 and 6, initiated at $t = 0.304$ s considering grid-islanded mode. Considering (DR#56) as a reference measurement, as seen in Fig. 5(b) and (d), both MLS and MKF identify the correct direction in less than 4ms, while DFT reaches correct identification after almost 50ms in both cases. Compared to DFT, calculations within an unsaturated interval make the MLS and MKF less susceptible to CT saturation effects.

B. High-Impedance Faults

High-impedance faults (HIFs) are challenging for conventional protection relays to detect due to their low-fault current magnitude. In addition, since HIFs accompany arcs, their waveforms are highly distorted, containing high-order harmonics. To evaluate the capabilities of the two proposed directional frameworks, the distortion-controllable HIF model

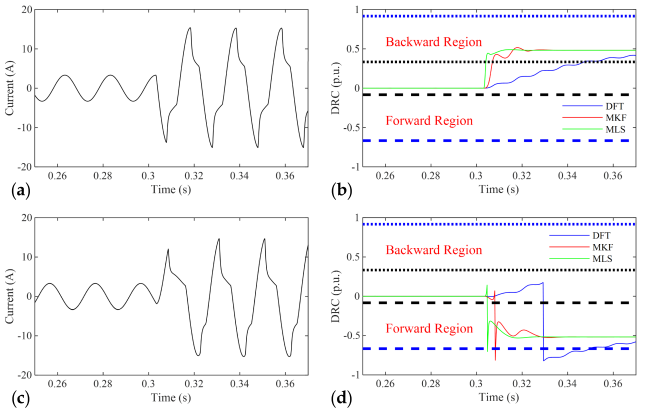

Fig. 5. Performance of the fault direction detection algorithm under CT saturation. (a) Fault current signal for 3LG fault between buses 3 and 5. (b) Calculated DRC via different frameworks for 3LG fault between buses 3 and 5. (c) Fault current signal for 2LG fault between buses 5 and 6. (d) Calculated DRC via different frameworks for 2LG fault between buses 5 and 6.

TABLE IV
CONDITIONS OF CASE STUDIES

Case	Fault Location	Condition Modeling	Parameters			
			OFS (kV)	EXT (kΩ)	DUR (ms)	RT (kΩ)
1	B5-B6	Dry Grass	6.488	0.904	10.3	100
2	B3-B5	Wet Soil	5.523	4.241	8.56	100

has been used for simulation cases. The distortion-controllable model effectively reflects the nonlinearity of the HIFs based on different materials and humidity conditions [35]. This model is characterized by four parameters, including OFS, EXT, DUR, and RT, corresponding to offset, extension of distortions, duration, and impedance, respectively. More than 100 HIF scenarios are generated and applied to the algorithms. For conciseness, only two scenarios are introduced in Table IV in grid-connected mode. With (DR#56) as measurement reference, Fig. 6 shows that all algorithms have correctly identified the fault direction for HIFs. However, in both scenarios, the MLS algorithm achieves the correct identification after 2.5 and 3 ms corresponding to forward and backward faults. The time required for correct direction identification by MKF and DFT algorithms is around 12.5 and 16.5 ms respective to forward and backward faults.

C. Faults Near Rotational Generators

As explained in the Introduction, in case of a short circuit close to a generator (i.e., SG or IG, DFIG), the sinusoidal part of the fault current may not remain constant-magnitude. Furthermore, the frequency can also vary, especially for IGs and DFIGs [23]. In such cases, directional algorithms may operate with large delays or even incorrectly since the actual fault current may not be similar to the standard waveform in (1) [9]. Two fault scenarios are given for faults near generators. In the first scenario, as shown in Fig. 7(a) and (b), an LG fault is applied close to the DFIG at $t = 0.3$ s in grid-islanded mode. Taking DR#56 relay as the reference,

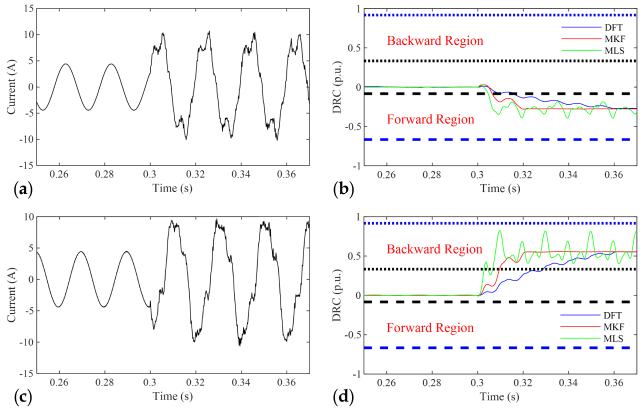

Fig. 6. Performance of the fault direction algorithms under HIF conditions. (a) Current signal of HIF for Case 1. (b) DRC for Case 1. (c) Current signal of HIF for Case 2. (d) DRC for Case 2.

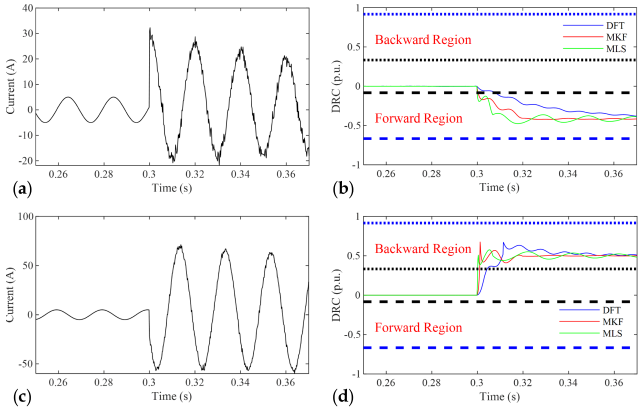

Fig. 7. Performance of the fault direction algorithms under fault close to DG. (a) Current signal of SLG fault close to DFIG. (b) DRC for fault close to DFIG measured through DR#56. (c) Current signal of SLG fault close to SG. (d) DRC for fault close to SG measured through DR#56.

Fig. 7(b) shows that the MLS and MKF can correctly identify the fault direction after 2.5 ms, while DFT reaches correct direction identification after 9 ms. For another case, as shown in Fig. 7(a), the same fault condition is applied close to the SG in grid-connected mode. As can be seen in Fig. 7(b), MLS and MKF can correctly identify the fault direction in 2 ms, while DFT identifies the correct direction after 6 ms.

D. Effect of Isolated Neutral

The neutral points in the test system in Fig. 3 have been assumed to be solidly connected to the ground. To verify the performance of the proposed algorithms for isolated-neutral networks, all the neutral connections to the ground were removed, and the proposed methods were tested for two forward and backward SLG fault scenarios. In the first case, an SLG short-circuit fault was considered between buses 3 and 5 with the resistance of 50 Ω, initiated at $t = 0.3$ s. The results from this case are shown in Fig. 8(a) and (b). As it can be seen in Fig. 8(a), the short-circuit current is not exactly sinusoidal; rather, it has obvious distortions. Nevertheless, according to Fig. 8(b), the proposed methods can detect the fault direction. While the MLS shows

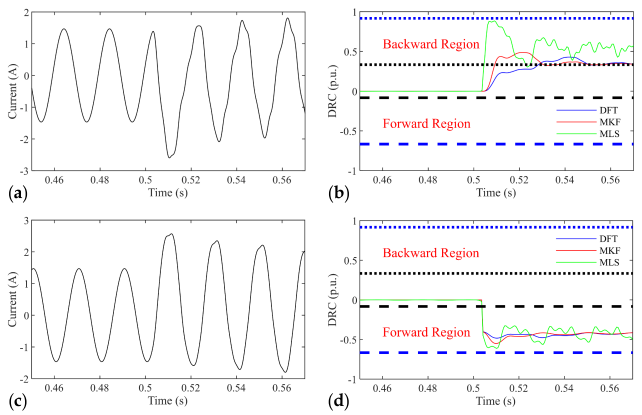

Fig. 8. Performance of the fault direction algorithms in case of single line to ground fault in ungrounded test system. (a) Current signal of SLG fault between buses 3 and 5. (b) DRC for SLG fault between buses 3 and 5. (c) Current signal of SLG fault between buses 5 and 6. (d) DRC for SLG fault between buses 5 and 6.

to be superior in terms of speed, the MKF algorithm has a more stable performance with a bit longer respective delay. For the second scenario, an SLG short-circuit fault was considered in the line between buses 5 and 6, occurring at $t = 0.3$ s. The resistance of the fault is set to 50 Ω, and the results are shown in Fig. 8(c) and (d). Similarly, as shown in Fig. 8(c), the short-circuit current is not exactly sinusoidal, and it is distorted. However, Fig. 8(d) shows that the proposed methods can detect the fault direction. Similar to the previous case, the performance of MLS is superior in terms of speed, while MKF has a more stable performance with a bit more delay.

V. Field Recorded Data

To evaluate the performance of the proposed directional algorithm in real-world conditions by taking into account noise effects, field-recorded data from real events have been fed to the proposed algorithm. The single line diagram in Fig. 9 partly represents a natural liquid gas refinery plant. In Fig. 9, T#1 refers to the incoming transformer, with the voltage level of 33/11kV and, T#2 refers to the low-voltage transformer, with the voltage levels 11/0.4kV. It is worth mentioning that the neutrals in this network are grounded, where the star sides of the T#1 transformers (YD) are connected to the ground via a resistance equal to 7.8 Ω, while the star sides of T#2 transformers (DY) are solidly grounded. A great share of the loads shown in Fig. 9 are induction machines. As shown in Fig. 9, the data have been collected through a 7SJ80 multifunction protection relay installed close to a diesel generator (DG) bus. This relay can measure instantaneous values of currents and voltage signals in intervals of 1 ms. This means that for a frequency of 50 Hz, the relay can record 20 samples/cycle.

As shown in Fig. 10, MLS, MKF, and DFT can correctly identify the forward direction, respectively in 4.5, 13, and 21 ms after fault inception. For backward faults, the MLS, MKF, and DFT can correctly identify the direction in respectively 2.5, 8.5, and 14.5 ms after fault inception under noise. Additionally, as shown in Fig. 11, MLS and MKF can swiftly identify fault direction using sub-cycle data, whereas DFT

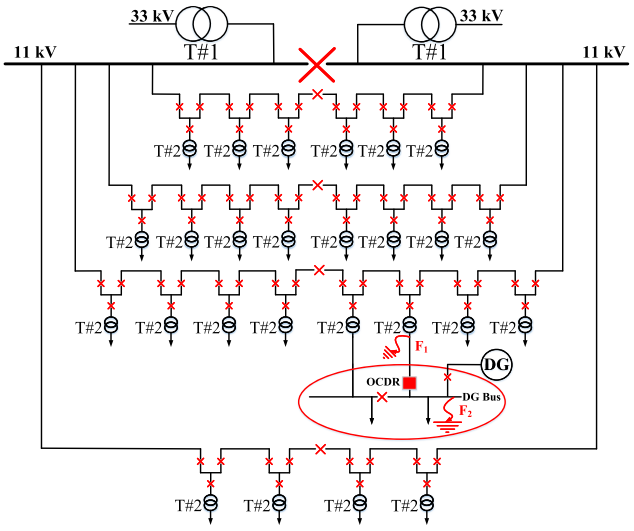

Fig. 9. Single line diagram of a real distribution grid including a DG unit.

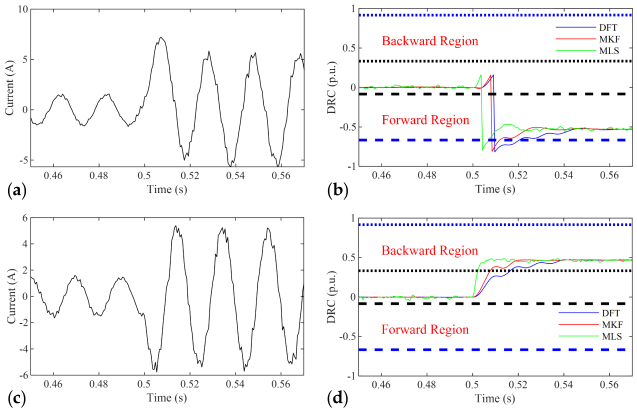

Fig. 10. Performance of the fault direction algorithms using field recorded data. (a) Current signal for SLG fault at F1. (b) DRC for the fault at F1. (c) Current signal for SLG fault at F2. (d) DRC for the fault at F2.

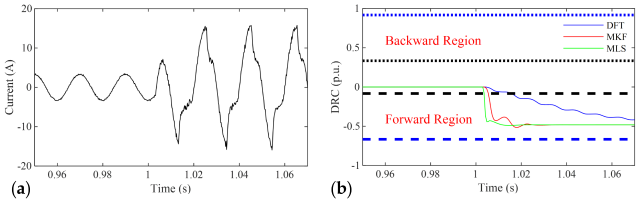

Fig. 11. Performance of the fault direction algorithms using field recorded data. (a) Saturated current signal for three phase to ground fault at F1. (b) DRC for the fault at F1.

involves long delays to achieve the correct result. Notably, the MLS has a faster response time compared to all algorithms.

VI. Performance Comparison

The performance of the proposed directional identification index is compared with the previously published algorithms. The algorithms are compared for 2000 fault scenarios by considering CT saturation, HIFs, difference FRs, and near-generator faults. The algorithms are briefly described in the following.

1) *Method 1 (M1):* This method is based on the rate of change of superimposed components of voltage (Δv) and current (Δi) [7]. A forward fault is identified when Δv and Δi superimposed components have opposite signs, and a backward fault if they have the same sign. Note that Δv and Δi are calculated using three consecutive moving windows with the length of 8 cycle.
2) *Method 2 (M2):* This method is based on the multiplication of prefault current and the rate of change of fault current, as introduced in [8]. The obtained index is then fed to a half-cycle moving average filter. The index was shown to have strict behavior for forward and backward faults. The index identifies forward fault if the index varies between 0.25 and 1 and backward fault if the index varies between -0.25 and -1.
3) *Method 3 (M3):* This method was introduced in [10], proposing an index based on the cumulative instantaneous frequency. During normal operation, the index is zero. For a forward fault, the index becomes strictly negative, while for a backward fault, the index becomes strictly positive. This method requires half-cycle measurement data for the calculation of instantaneous frequency.
4) *Method 4 (M4):* In this method, which was first proposed in [9], it was demonstrated that the similarity between the prefault and postfault current is much higher for forward faults than for backward faults. Accordingly, a relation-based algorithm was developed, where a forward fault is identified when the correlation coefficients range from 0 to 0.8, and a backward fault is identified when the correlation coefficients range from -0.2 to -1. Note that the length of the data window plays an important role in the accuracy and the response time of this method.

The performances of the direction identification algorithms are compared by applying 500 scenarios of different FTs, FRs, HIFs, CT saturation conditions, and faults close to DGs while considering Gaussian noise with signal-to-noise ratios (SNRs) ranging between 30 and 50. The average time response and the correct number of identifications are summarized in Table V. From Table V, it is concluded as follows.

1) *Method 1:* While this method can deal with faults without CT saturation, due to its dependency on the wave shape, its performance is poor for HIFs, faults accompanied by CT saturation, and faults close to DGs. The average response time of this method is 30.4 ms, and the percentage of its correct direction identification is 61.7%.
2) *Method 2:* This method shows acceptable performance under noisy conditions and for faults without CT saturation. However, this method is challenged during HIFs, faults with CT saturation, and faults close to DGs, making its response time increase significantly. The percentage of correct identifications for this algorithm is 79.6% and its average response time is about 28.4 ms.
3) *Method 3:* This method deals with faults without CT saturation and faults close to DGs; however, its performance degrades under CT saturation and HIFs for

TABLE V
ACCURACY OF THE ALGORITHMS

Method		Correct Identification (%)	Average Response Time (ms)
M1		61.7	30.4
M2		79.6	28.4
M3		86.1	17.1
M4		89.6	19.7
Proposed Algorithms	DFT	90.2	25.6
	MKF	94.4	10.8
	MLS	100	3.5

its frequency estimation scheme dependence on wave shape. Normally, this method has a response time of 17.1 ms and a correct direction identification rate of 86.1%.

4) *Method 4:* This method can deal with faults without CT saturation, HIFs, and faults close to DGs; however, its performance deteriorates during CT saturation. Its average response time is approximately 19.7 ms, and its rate of correct direction identification is 89.6%.
5) *Proposed algorithm using DFT:* This algorithm can deal with faults without CT saturation and low decaying dc, HIFs, and faults close to DGs, however, under high decaying dc and deep CT saturation, it experiences large delays. It has an average response time of 25.6 ms and a rate of correct direction identification of 90.2%.
6) *Proposed algorithm using MKF:* This algorithm can deal with faults with/without CT saturation, HIFs, and faults close to DGs; however, its performance degrades in case of high decaying dc. With an average response time of about 10.8 ms, it identifies 94.4% of scenarios correctly.
7) *Proposed algorithm using MLS:* This method can deal with faults with/without CT saturation, HIFs, and faults close to DGs. Compared to other methods, MLS has no significant sensitivity to high amounts of decaying dc. This scheme has an average response time of 3.5 ms and can identify the correct direction for all the scenarios.

VII. CONCLUSION

Increased use of distributed generations in the electrical power system has become challenging concerning protection strategies. On one hand, these sources may increase the short-circuit fault currents, leading to an increased possibility of CT saturation. On the other hand, the presence of DGs may result in the alteration of fault current direction, causing issues with the protection zones of relays. To tackle these challenges, new frameworks for fault direction identification in MV distribution grids were investigated in this article, with an emphasis on immunity to CT saturation effects. This end was attained by developing a novel protection algorithm, realized via two separate computational frameworks: a MLS technique and a MKF. These frameworks are comprehensive and straightforward, ensuring fast response times, high accuracy, and robustness in the presence of decaying dc offset, CT saturation, and noisy conditions. Extensive performance evaluations were carried out considering different types of DGs, neutral grounding arrangements, FTs, FLs, and FRs with the help of simulation and experimental scenarios. The results indicated that MKF performs well for most scenarios and reaches almost 94% correct identification within 11 ms time response. However, the MLS-based algorithm is superior and robust in identifying the fault direction within 4 ms, even under CT saturation. Besides, both algorithms are robust under linear and nonlinear high-impedance fault conditions. Compared to the state-of-the-art algorithms, the proposed frameworks demonstrate notable precision, speed, and noise immunity. From the simulation and experimental results, it can be concluded that the proposed frameworks effectively identify the fault direction under various challenging conditions with high accuracy and fast response time.

REFERENCES

[1] N. El-Naily, S. M. Saad, A. Elhaffar, E. Zarour, and F. Alasali, "Innovative adaptive protection approach to maximize the security and performance of phase/earth overcurrent relay for microgrid considering Earth fault scenarios," *Electr. Power Syst. Res.*, vol. 206, May 2022, Art. no. 107844, doi: 10.1016/j.epsr.2022.107844.

[2] A. Y. Hatata, A. S. Ebeid, and M. M. El-Saadawi, "Optimal restoration of directional overcurrent protection coordination for meshed distribution system integrated with DGs based on FCLs and adaptive relays," *Electr. Power Syst. Res.*, vol. 205, Apr. 2022, Art. no. 107738, doi: 10.1016/j.epsr.2021.107738.

[3] G. Suryanarayana, G. K. Rao, S. Sarangi, and P. Raja, "Directional relaying using parameter estimation approach," *Int. J. Electr. Power Energy Syst.*, vol. 107, pp. 597–604, May 2019, doi: 10.1016/j.ijepes.2018.12.003.

[4] H. H. Zeineldin, H. M. Sharaf, D. K. Ibrahim, and E. E.-D.-A. El-Zahab, "Optimal protection coordination for meshed distribution systems with DG using dual setting directional over-current relays," *IEEE Trans. Smart Grid*, vol. 6, no. 1, pp. 115–123, Jan. 2015, doi: 10.1109/TSG.2014.2357813.

[5] M. Yousaf, A. Jalilian, K. M. Muttaqi, and D. Sutanto, "An adaptive overcurrent protection scheme for dual-setting directional recloser and fuse coordination in unbalanced distribution networks with distributed generation," *IEEE Trans. Ind. Appl.*, vol. 58, no. 2, pp. 1831–1842, Mar. 2022, doi: 10.1109/TIA.2022.3146095.

[6] S. S. Fatemi and H. Samet, "Considering DGs voltage protection in optimal coordination of directional overcurrent relays to minimize the energy not supplied," *IEEE Syst. J.*, vol. 15, no. 3, pp. 4037–4045, Sep. 2021, doi: 10.1109/JSYST.2020.3001378.

[7] P. Jafarian and M. Sanaye-Pasand, "High-speed superimposed-based protection of series-compensated transmission lines," *IET Gener., Transmiss. Distrib.*, vol. 5, no. 12, pp. 1290–1300, 2011, doi: 10.1049/iet-gtd.2011.0293.

[8] M. M. Eissa and M. M. A. Mahfouz, "New high-voltage directional and phase selection protection technique based on real power system data," *IET Gener., Transmiss. Distrib.*, vol. 6, no. 11, pp. 1075–1085, Nov. 2012, doi: 10.1049/iet-gtd.2012.0319.

[9] M. S. Payam, H. Samet, T. Ghanbari, and M. Tajdinian, "Fault direction identification utilizing new current-based index founded on rate of change of fault current," *Electr. Power Syst. Res.*, vol. 201, Dec. 2021, Art. no. 107511, doi: 10.1016/j.epsr.2021.107511.

[10] M. S. Payam, H. Samet, and T. Ghanbari, "Instantaneous frequency-based algorithm for directional relays," *IEEE Syst. J.*, vol. 15, no. 2, pp. 2642–2652, Jun. 2021, doi: 10.1109/JSYST.2020.3029849.

[11] S. Akter, S. Biswal, N. S. Rathore, P. Das, and A. Y. Abdelaziz, "Amplitude based directional relaying scheme for UPFC compensated line during single pole tripping," *Electr. Power Syst. Res.*, vol. 184, Jul. 2020, Art. no. 106290, doi: 10.1016/j.epsr.2020.106290.

[12] P. Jena and A. K. Pradhan, "Directional relaying during single-pole tripping using phase change in negative-sequence current," *IEEE Trans. Power Del.*, vol. 28, no. 3, pp. 1548–1557, Jul. 2013, doi: 10.1109/TPWRD.2013.2258687.

[13] Q. Lai, Z. Zhang, K. Xu, and X. Yin, "A new method of fault direction identification for different types of renewable energy source integrations," *IEEE Trans. Power Del.*, vol. 37, no. 4, pp. 2932–2941, Aug. 2022, doi: 10.1109/TPWRD.2021.3119356.

[14] P. Jafarian and M. Sanaye-Pasand, "A traveling-wave-based protection technique using wavelet/PCA analysis," *IEEE Trans. Power Del.*, vol. 25, no. 2, pp. 588–599, Apr. 2010, doi: 10.1109/TPWRD.2009.2037819.

[15] S. P. Valsan and K. S. Swarup, "Wavelet transform based digital protection for transmission lines," *Int. J. Electr. Power Energy Syst.*, vol. 31, nos. 7–8, pp. 379–388, Sep. 2009, doi: 10.1016/j.ijepes.2009.03.024.

[16] W. Chen, O. P. Malik, X. Yin, D. Chen, and Z. Zhang, "Study of wavelet-based ultra high speed directional transmission line protection," *IEEE Trans. Power Del.*, vol. 18, no. 4, pp. 1134–1139, Oct. 2003, doi: 10.1109/TPWRD.2003.817511.

[17] D. Mu, S. Lin, H. Zhang, and T. Zheng, "A novel fault identification method for HVDC converter station section based on energy relative entropy," *IEEE Trans. Instrum. Meas.*, vol. 71, pp. 1–10, 2022, doi: 10.1109/TIM.2022.3157374.

[18] N. Shahbazi, S. Bagheri, and G. B. Gharehpetian, "Performance improvement of transformer differential protection during cross-country fault using hyperbolic S-transform," *IEEE Trans. Instrum. Meas.*, vol. 71, pp. 1–9, 2022, doi: 10.1109/TIM.2021.3128691.

[19] N. Zhang and M. Kezunovic, "Transmission line boundary protection using wavelet transform and neural network," *IEEE Trans. Power Del.*, vol. 22, no. 2, pp. 859–869, Apr. 2007, doi: 10.1109/TPWRD.2007.893596.

[20] U. Lahiri, A. K. Pradhan, and S. Mukhopadhyaya, "Modular neural network-based directional relay for transmission line protection," *IEEE Trans. Power Syst.*, vol. 20, no. 4, pp. 2154–2155, Nov. 2005, doi: 10.1109/TPWRS.2005.857839.

[21] T. S. Sidhu, H. Singh, and M. S. Sachdev, "Design, implementation and testing of an artificial neural network based fault direction discriminator for protecting transmission lines," *IEEE Trans. Power Del.*, vol. 10, no. 2, pp. 697–706, Apr. 1995, doi: 10.1109/61.400862.

[22] W. Li, A. Monti, and F. Ponci, "Fault detection and classification in medium voltage DC shipboard power systems with wavelets and artificial neural networks," *IEEE Trans. Instrum. Meas.*, vol. 63, no. 11, pp. 2651–2665, Nov. 2014, doi: 10.1109/TIM.2014.2313035.

[23] N. Tleis, *Power Systems Modelling and Fault Analysis: Theory and Practice*, 2nd ed., San Diego, CA, USA: Academic, 2019.

[24] S. Tohidi and M.-I. Behnam, "A comprehensive review of low voltage ride through of doubly fed induction wind generators," *Renew. Sustain. Energy Rev.*, vol. 57, pp. 412–419, May 2016, doi: 10.1016/j.rser.2015.12.155.

[25] A. M. Howlader and T. Senjyu, "A comprehensive review of low voltage ride through capability strategies for the wind energy conversion systems," *Renew. Sustain. Energy Rev.*, vol. 56, pp. 643–658, Apr. 2016, doi: 10.1016/j.rser.2015.11.073.

[26] S. K. Salman and A. T. Johns, *Digital Protection for Power Systems*, 2nd ed., Stevenage, U.K.: Institution of Engineering and Technology, 2023.

[27] M. Tajdinian, H. Samet, and Z. M. Ali, "Differential protection algorithm founded on Kalman filter-based phase tracking," *IEEE Trans. Instrum. Meas.*, vol. 71, pp. 1–9, 2022, doi: 10.1109/TIM.2021.3137565.

[28] A. G. Phadke and J. S. Thorp, *Computer Relaying for Power Systems*, 2nd ed., Hoboken, NJ, USA: Wiley, 2009.

[29] B. Behdani, M. Tajdinian, M. Allahbakhshi, M. Popov, M. Shafie-Khah, and J. P. S. Catalão, "Experimentally validated extended Kalman filter approach for geomagnetically induced current measurement," *IEEE Trans. Ind. Electron.*, vol. 69, no. 6, pp. 6316–6328, Jun. 2022, doi: 10.1109/TIE.2021.3094488.

[30] The MathWorks, Inc. (2022). *MATLAB version: 9.13.0 (R2022b)*. [Online]. Available: https://www.mathworks.com

[31] S. Kar, S. R. Samantaray, and M. D. Zadeh, "Data-mining model based intelligent differential microgrid protection scheme," *IEEE Syst. J.*, vol. 11, no. 2, pp. 1161–1169, Jun. 2017, doi: 10.1109/JSYST.2014.2380432.

[32] S. Casoria, G. Sybille, and P. Brunelle, "Hysteresis modeling in the MATLAB/Power system blockset," *Math. Comput. Simul.*, vol. 63, nos. 3–5, pp. 237–248, Nov. 2003, doi: 10.1016/s0378-4754(03)00070-3.

[33] J. G. Frame, N. Mohan, and T.-h. Liu, "Hysteresis modeling in an electro-magnetic transients program," *IEEE Power Eng. Rev.*, vol. PER-2, no. 9, pp. 59–60, Sep. 1982, doi: 10.1109/MPER.1982.5519502.

[34] M. Tajdinian, M. Allahbakhshi, A. Bagheri, H. Samet, P. Dehghanian, and O. Parkash Malik, "An enhanced sub-cycle statistical algorithm for inrush and fault currents classification in differential protection schemes," *Int. J. Electr. Power Energy Syst.*, vol. 119, Jul. 2020, Art. no. 105939, doi: 10.1016/j.ijepes.2020.105939.

[35] M. Wei, W. Liu, F. Shi, H. Zhang, Z. Jin, and W. Chen, "Distortion-controllable arc modeling for high impedance arc fault in the distribution network," *IEEE Trans. Power Del.*, vol. 36, no. 1, pp. 52–63, Feb. 2021, doi: 10.1109/TPWRD.2020.2981376.

Mohsen Tajdinian received the Ph.D. degree in electrical engineering from Shiraz University, Shiraz, Iran, in 2020.

Currently, he is a Research and Development Scientist with Hitachi Energy Research, Västerås, Sweden. His research interests include power system protection, power system control, stability and security, power quality, and high-voltage products.

Behzad Behdani (Member, IEEE) received the M.Sc. degree in electrical power systems engineering from Shiraz University, Shiraz, Iran, in 2020. He is currently pursuing the Ph.D. degree in electrical power engineering with Delft University of Technology, Delft, The Netherlands.

Mr. Behdani is recognized as a Top Elite National Talent by Iran's National Elites Foundation (INEF) in 2020.

Md Tanbhir Hoq received the Ph.D. degree from the Royal Institute of Technology (KTH), Stockholm, Sweden, in 2023, where he worked on protecting high-voltage series-compensated lines.

He was a Scientist at Hitachi Energy Research, Västerås, Sweden, where he is currently the Research Team Manager.

Marjan Popov (Fellow, IEEE) received the Ph.D. degree in electrical power engineering from Delft University of Technology, Delft, The Netherlands, in 2002.

He is a Professor of power system protection at Delft University of Technology.

Prof. Popov received the prestigious Dutch Hidde Nijland Prize for Extraordinary Research Achievements in 2010, the IEEE PES Prize Paper Award, and the IEEE Switchgear Committee Award in 2011.